Iris Recognition Using a Novel Segmentation Method and Fuzzy ARTMAP Neural Network

Arash Taherian[1], Mahdi Aliyari Sh.[2]
1- Department of Electrical and Computer Engineering, Islamic Azad University, South Tehran Branch, Tehran, Iran.
Email: taherian_arash@yahoo.com
2- Faculty of Electrical and Computer Engineering, K. N. Toosi University of Technology, Tehran, Iran.
Email: aliyari@eetd.kntu.ac.ir

Received: June 2012 Revised: October 2012 Accepted: November 2012

ABSTRACT:
A biometric system provides automatic identification of an individual based on unique features or characteristics possessed by that person. Iris recognition is regarded as one of the most reliable and accurate available biometric systems. This paper proposes an efficient iris recognition system that employs a novel method to localize the iris region on the eye image based on approximating the iris radius using the pupil characteristics and cumulative sum based gray change analysis technique to extract features from the normalized iris template. Fuzzy ARTMAP neural network is also applied to classify the iris codes. The results of simulations on a set of 756 eye images illustrated a fast, accurate and noise resistant personal identification system. The proposed system achieved zero false acceptance rate using 1800-bit binary iris codes and recognized all authorized users with 100% accuracy.

KEYWORDS: Biometrics, Fuzzy ARTMAP Neural Network, Iris Recognition, Segmentation.

1. INTRODUCTION

Biometrics technology plays an important role in public security and information security domains. Using various physiological characteristics of human, such as speech, fingerprint, hand geometry, face, iris, retina, etc., biometrics accurately identifies everyone and distinguishes one from another [1].

Iris recognition is one of the important biometric approaches in human identification and has become a very active topic in research and practical application. Iris region is the area between the pupil and the sclera. Since, it is made of many minute characteristics; this field is sometimes called iris texture [2]. These visible characteristics are not only unique for each subject, but also unique for each eye of a subject and remain almost stable from six months of age to death. Such unique feature in the anatomical structure of the iris facilitates the differentiation among individuals [3].

Compared with other biometric features, iris patterns are more stable and reliable and unrelated to health or the environment. Iris recognition systems are noninvasive to their users, but do require a cooperative subject. Because of such unique features, iris recognition has become one of the most reliable and acceptable biometric approaches among users [4].

Iris recognition system consists of image acquisition, localization of the iris region in a digital eye image, feature extraction from normalized and enhanced iris template, and classification of iris codes [5].

A variety of techniques have been developed for iris localization. In [3, 6-10], the system with the circular edge detector, and in [11] a gradient based Hough transform are used for the localizing of the iris. Furthermore, circular Hough transform [12, 13], and random Hough transform are applied to find the iris circles and complete the iris localization. In [11, 14] Canny operator is used to locate the pupil boundary. These methods need a long time to locate iris; in this paper, a fast iris localization algorithm is proposed.

For feature extraction and pattern matching processes, various algorithms have been also applied. These methods use local and global features of the iris. Using phase based approach [3, 6-10], wavelet transform zero crossing approach [15, 16], Gabor filtering [14], and texture analysis based methods [12, 14-19] the solving of the iris recognition problem is considered. In [20-22], independent component analysis is proposed for iris recognition. Daugman [3, 6-10] used multiscale quadrature wavelets to extract texture phase structure information of the iris to generate a 2048-bit iris code and compared the difference between a pair of iris representations by computing their Hamming distance. Boles and Boashash [15] calculated a zero-crossing representation of 1D wavelet transform at various resolution levels of a concentric circle on an iris image to characterize the texture of the iris. Iris matching was based on two dissimilarity functions. Sanchez-Avila and Sanchez-

Reillo [16] further developed the method of Boles and Boashash by using different distance measures, such as Euclidean distance and Hamming distance, for matching. Wildes et al. [12] represented the iris texture with a Laplacian pyramid constructed with four different resolution levels and used the normalized correlation to determine whether the input image and the model image are from the same class. In this paper, a combination of fast and noise resistant methods is used for feature extraction and classification of iris codes.

2. IRIS RECOGNITION PROCESS

Identification process begins with the eye image acquisition; this stage includes the near-infrared (NIR) lighting system, the positioning system and the physical capture system. Images are captured and saved in grayscale format and then are presented in the system. In this case, an 8-bit code presents the brightness of each pixel; consequently, the resulting image will be composed of the gray shades. Pre-processing of the captured image is the next step; this stage includes iris localization, normalization and enhancement of the normalized iris template by illumination compensation and contrast enhancement techniques. To compare these normalized templates, textural features are extracted. Data obtained from the images should prepare appropriate Criterion for identification and differentiation between the patterns and also must be compressed as much as possible to minimize the required memory for data storage and to increase the speed of the authentication process [23].

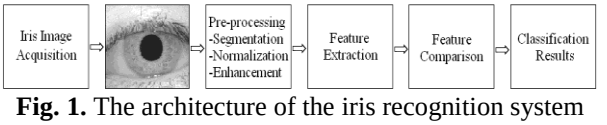

Fig. 1. The architecture of the iris recognition system

Although various techniques have been designed to locate the iris region but the most important algorithms that are applied in most studies have been proposed by Daugman and Wildes.

In Daugman's method, pupillary and limbic boundaries of the eye have been approximated as non-concentric circles. Thus, a boundary could be described by three parameters: radius *r*, and the coordinates of the center of the circle (x_c , y_c). He proposed an integro-differential operator for detecting the iris boundary by searching the parameter space.

$$\max(r, x_c, y_c) \left| G_\sigma(r) * \frac{\partial}{\partial r} \oint_{r, x_c, y_c} \frac{\mathbf{I}(x,y)}{2\pi r} ds \right| \quad (1)$$

where $G_\sigma(r)$ is a smoothing function such as a Gaussian of scale σ and $\mathbf{I}(x,y)$ is the original image of the eye. The complete operator behaves as a circular edge detector that searches over the candidate domain iteratively with respect to increasing radius *r* for maximum contour integral derivative [3, 6-10].

Wildes employed an automatic segmentation algorithm based on the circular Hough transform to locate the iris region. In his method, first, an edge map is generated by calculating the first derivatives of intensity values in an eye image and then thresholding the result. From the edge map, votes are cast in Hough space for the parameters of circles passing through each edge point [11-13]. These parameters are the centre coordinates (x_c , y_c), and the radius *r*, which are able to define any circle according to equation (2).

$$x_c^2 + y_c^2 - r^2 = 0 \quad (2)$$

In this paper, a novel method is proposed to localize the iris region on the eye image based on approximating the iris radius using the pupil characteristics. In addition to fast performance, this method also can detect the iris boundaries accurately.

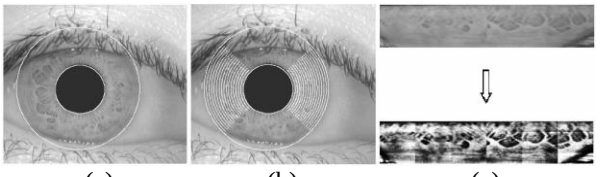

(a) (b) (c)

Fig. 2. Image Pre-processing: (a) Localization of the iris region, (b) Unwrapping and normalization, (c) Enhancement of the normalized iris template

After region of the iris is isolated from the eye image, this region is transformed to a normalized rectangular template using Daugman's rubber sheet model. This method remaps each point within the iris region to a pair of polar coordinates (r,θ) in order to produce a normalized representation with constant dimensions. The remapping of the iris region is modeled as below.

$$\mathbf{I}(x(r,\theta), y(r,\theta)) \rightarrow \mathbf{I}(r,\theta) \quad (3)$$

where $\theta \in ([3\pi/4, 5\pi/4] \cup [7\pi/4, 9\pi/4])$ is the sampling angle and $r \in [0,1]$ is the normalized distance between each sampling point and the pupillary boundary according to the iris width in each angle [11].

After completing the pre-processing stage by enhancing the normalized iris template using illumination compensation and histogram equalization techniques, cumulative sum based gray change analysis method is used for extracting features and encoding the produced image. This algorithm generates iris codes by analyzing the changes of gray values of iris patterns. Upward slope of cumulative sums means that iris pattern may change from darkness to brightness; downward slope of cumulative sums means the opposite change of upward slope [24]. Overall feature extraction process is as follows.

Step 1. Divide normalized iris image into basic cell regions for calculating cumulative sums. One cell

region has m × n pixels size. An average gray value is used as a representative value of a basic cell region to calculate the cumulative sum.

Step 2. Basic cell regions are grouped horizontally and vertically as shown in figure 3.

Step 3. Calculate cumulative sums over each group.

Step 4. Generate iris feature codes.

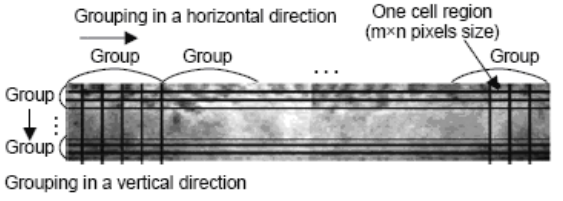

Fig. 3. Division of normalized iris image into cell regions and grouping of cell regions [25]

Cumulative sums are calculated as follows. Suppose that X_1, X_2, ... , X_5 are five representative values of each cell region within the first group located on the left top corner of figure 3.

- Calculate the average:
$$\overline{X} = (X_1 + X_2 + ... + X_5)/5 \quad (4)$$
- Calculate cumulative sum from 0: $S_0 = 0$.
- Calculate the other cumulative sums by adding the difference between the current value and the average to the previous sum:
$$S_i = S_{i-1} + (X_i - \overline{X}) \quad \text{for} \quad i = 1,2,...,5 \quad (5)$$

The cumulative sums begin from 0 and end at 0. After calculations, iris codes are generated in each cell by analyzing sums [25]. The iris code is set to 1 for cells that located on the upward slope (left side of the MAX value or right side of the MIN value) and is set to 0 for others [24].

During enrollment, the system saves encoded features into a database. During authentication, after performing pre-process steps like enrollment stage and extracting features, the system compares the presented iris against all database codes to verify a claimed identity or identify an individual. There are different algorithms to compare the input code with the codes saved to the database of the identification system; among them, calculating the Hamming distance is the most common method used for measuring the similarity between the binary codes. A lower Hamming distance indicates higher similarity.

$$HD = \frac{1}{N}\left(\sum_{i=1}^{N} A_i \oplus B_i\right) \quad (6)$$

where A_i and B_i denote the enrolled iris code and the new input code respectively; N is the total number of cells and $\oplus$ is the XOR operator [11].

One of the other techniques that applied in this purpose is the neural network; in this regard, networks with parallel combination of several Rosenblatt's perceptrons [4] and networks with multi-layer perceptron (MLP) architecture [5] are used in pervious studies.

While the noise resistance of the MLP networks is weak, and they are usually unable to classify the noisy patterns correctly, many factors such as ambient lighting reflections, change in the angle of the user's head during image acquisition process or occlusions like eyelashes or eyelids or even the use of contact lenses cause noise in the input images.

In this paper, a combination of the cumulative sum based gray change analysis method for encoding the iris patterns and fuzzy ARTMAP neural networks for comparing the iris codes is used to deal with the input noise. Although the algorithm of the feature extraction method consists of simple calculations, but the obtained codes have good resistance against the input noise; fast learning ability and high noise resistance, also make fuzzy ARTMAP neural networks one of the best options for pattern classification purposes.

Fuzzy ARTMAP, achieves a synthesis of fuzzy logic and Adaptive Resonance Theory (ART) neural networks by exploiting a close formal similarity between the computations of fuzzy subsethood and ART category choice, resonance and learning. Because this neural network architecture has a small number of parameters and requires no problem-specific system crafting or choice of initial weight values, it is also easy to use. Although off-line training of fuzzy ARTMAP by applying the shuffled training set exemplars in a number of epochs increases the classification accuracy of this network, where an epoch is defined as one cycle of training on an entire set of input exemplars, one way in which this kind of network differs from many previous fuzzy pattern recognition algorithms is incremental or on-line learning; it means that fuzzy ARTMAP is also able to learn each input as it is received on-line, rather than performing an off-line optimization of a criterion function [26].

Each ARTMAP system includes a pair of adaptive resonance theory modules (ART_a and ART_b) that create stable recognition categories in response to arbitrary sequences of input patterns; these modules are linked by an inner ART module F^{ab} (also called map field) which is to determine whether the correct mapping has been established from inputs to outputs. Each ART system includes a field, F_0, of nodes that represent a current input vector; a field, F_1 that receives both bottom-up input from F_0 and top-down input from a field, F_2 that represents the active category (Figure 4). Associated with each F_2 category node j ($j = 1,...,N$) is a vector $\boldsymbol{w}_j \equiv (w_{j1},...,w_{jM})$ of adaptive weights. Initially, $w_{j1}(0) = \cdots = w_{jM}(0) = 1$; then each category is said to be uncommitted. After a category is selected for coding it becomes committed [27].

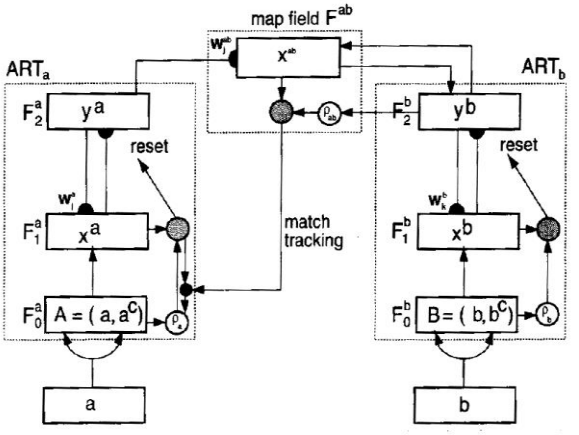

Fig. 4. Fuzzy ARTMAP architecture [26]

Adaptive resonance theory modules create recognition categories based on the training patterns presented in the system. ART_b is used for training ART_a and after completing the training phase, this module is discarded and the output is determined by applying the input patterns to ART_a. During supervised learning, ART_a receives a stream $\{\mathbf{a}^{(p)}\}$ of input patterns, and ART_b also receives a stream $\{\mathbf{b}^{(p)}\}$ of patterns, where $\mathbf{b}^{(p)}$ is the correct prediction given $\mathbf{a}^{(p)}$. These modules are linked by an internal controller that ensures autonomous system operation in real-time; the controller is designed to create the minimal number of ART_a recognition categories, needed to meet accuracy criteria [27].

The steps of fuzzy ARTMAP algorithm are summarized as follows.

1. Input data: The input pattern of ART_a is represented by the vector $\mathbf{a} = [a_1,...,a_{Ma}]$ and the input pattern of ART_b is represented by the vector $\mathbf{b} = [b_1,...,b_{Mb}]$ [26].

2. Parameters: There are three fundamental parameters corresponding to the performance and learning of fuzzy ART network [26].

- Choice parameter, ($\alpha > 0$): which acts on the category selection.
- Learning rate parameter, ($\beta \in [0,1]$): that controls the velocity of network adaptation.
- Vigilance parameter, ($\rho \in [0,1]$): that controls the network resonance. The vigilance parameter is responsible for the number of formed categories.

3. Algorithm structure:

- Complement coding is a normalization rule that preserves amplitude information and represents both on-response and off-response to an input vector. The complement coded input **I** to the field F_1 is the 2M-dimensional vector [26].

$$\mathbf{I} = (\mathbf{a}, \mathbf{a}^c) \equiv (a_1,..., a_M, a_1^c,..., a_M^c) \tag{7}$$

- For each input **I** and F_2 node j, the choice function T_j is defined by

$$T_j(\mathbf{I}) = \frac{|\mathbf{I} \wedge \mathbf{w}_j|}{\alpha + |\mathbf{w}_j|} \tag{8}$$

where the fuzzy AND operator $\wedge$ is defined by

$$(\mathbf{p} \wedge \mathbf{q})_i \equiv \min(p_i, q_i) \tag{9}$$

and where the norm $|\cdot|$ is defined by

$$|\mathbf{p}| \equiv \sum_{i=1}^{M} |p_i| \tag{10}$$

The system is said to make a category choice when at most one F_2 node can become active in a given time. The category choice is indexed by j, where $T_j = \max\{ T_j : j = 1...N \}$. If more than one T_j is maximal, the category j with the smallest index is chosen. In particular, nodes become committed in order $j = 1, 2, 3,....$ When the jth category is chosen, $y_j = 1$; and $y_i = 0$ for $i \neq j$ [26].

- Resonance occurs if the match function of the chosen category j, meets the vigilance criterion:

$$\frac{|\mathbf{I} \wedge \mathbf{w}_j|}{|\mathbf{I}|} \geq \rho \tag{11}$$

Otherwise, the value of the choice function T_j is set to zero for the duration of the input presentation to prevent the persistent selection of the same category during search. Then a new index j is chosen, and the search process continues until the chosen category satisfies (11) [26].

4. Learning: Once search ends, the weight vector $\boldsymbol{w}_j$ is updated. The adaptation of the ART_a and ART_b module weights is given by

$$\mathbf{w}_j^{(new)} = \beta(\mathbf{I} \wedge \mathbf{w}_j^{(old)}) + (1-\beta)\mathbf{w}_j^{(old)} \tag{12}$$

Fast learning corresponds to setting $\beta = 1$ [26].

5. MAP Field Activation: The map field F^{ab} is activated whenever one of the ART_a or ART_b categories is active. If the node j of F_2^a is chosen, then its weights $\boldsymbol{w}_j^{ab}$ activate F^{ab}. If the node k in F_2^b is active, then the node k in F^{ab} is activated by 1-to-1 pathways between F_2^b and F^{ab}. If both ART_a and ART_b are active, then F^{ab} becomes active only if ART_a predicts the same category as ART_b via the weights $\boldsymbol{w}_j^{ab}$. The F^{ab} output vector $\boldsymbol{x}^{ab}$ obeys

$$\boldsymbol{x}^{ab} = \begin{cases} \mathbf{y}^b \wedge \mathbf{w}_j^{ab} & \text{if the } j\text{th } F_2^a \text{ node is active and } F_2^b \text{ is active} \\ \mathbf{w}_j^{ab} & \text{if the } j\text{th } F_2^a \text{ node is active and } F_2^b \text{ is inactive} \\ \mathbf{y}^b & \text{if } F_2^a \text{ is inactive and } F_2^b \text{ is active} \\ \mathbf{0} & \text{if } F_2^a \text{ is inactive and } F_2^b \text{ is inactive [26].} \end{cases} \tag{13}$$

3. EYE IMAGE SEGMENTATION

In this section, the proposed localization algorithm will be described. The algorithm consists of two stages. In the first stage, the position of the pupil is detected as accurate as possible. In the second stage, the boundary circle between the iris and the sclera is detected.

3.1. Pupil Localization

Because the performance of this algorithm depends on the correct detection of center coordinates and radius of the pupil, initial estimates of location and size of this limb are obtained using the histogram analysis method, then these characteristics are determined more accurately using the Canny edge detector.

To obtain initial estimates, histogram of each eye image is plotted. The peak of this diagram shows the grayscale value of the pupil pixels; so, after converting other grayscale values to absolute white, the center coordinates of the pupil circle can be approximated by finding the row and the column with the minimum sum of grayscale values. In some cases, however, an image may have two peaks if there is significant glare from the eye lids, so in the first step grayscale values more than 200 are discarded from each diagram. An approximation of the pupil radius can also be calculated using equation (14),

$$r = \sqrt{\frac{N}{\pi}} \tag{14}$$

where N is the total number of pixels that detected inside the pupil region and r is the pupil radius.

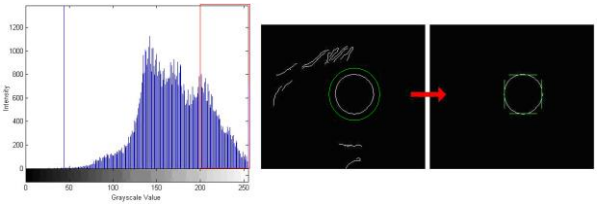

(a) (b)

Fig. 5. Pupil localization: (a) Eye image histogram; the largest number of pixels has a grayscale value of around 40, which corresponds to the pupil. (b) Pupil boundary determination using the Canny edge detector

In the next step, the Canny edge detector is used to improve pupil localization accuracy. First, the edges of the eye image map is produced by adjusting the maximum sensitivity threshold of the edge detector on 0.71 and a circle is assumed across the pupil with the center coordinates equal to the approximated pupil center coordinates and a radius with 10 pixels bigger than the approximated pupil radius; afterwards, points on the edges map that placed around the circumference of the assumed circle or outside of the circle are removed. Thereupon, an edges map is obtained, which mainly consists of the pupil boundary points and so, the pupil edges can be determined by finding rows and columns with the maximum number of ones. After detection of the edges, the pupil center coordinates can be calculated as half the distance between cross edges and its radius can be determined from equation (15).

$$r_p = \frac{1}{4}[(X_r - X_l) + (Y_b - Y_t)] \tag{15}$$

where r_p is the pupil radius, X_r and X_l are the horizontal coordinates of the right and the left points of the edge, Y_b and Y_t are the vertical coordinates of the bottom and the top points of the edge, respectively.

At the end of this stage, the estimated values are compared with the exact values obtained from the edge detector and if the difference is equal or more than 10, then the initially estimated values are used.

3.2. Limbic Boundary Detection

Existing methods for determining the border between iris and sclera are usually sensitive to ambient lighting levels and occlusions in the eye image such as eyelashes or eyelids. In the proposed method, the outer border of the iris is estimated using the pupil radius and the region of interest (ROI) for detecting the limbic boundary is determined using this estimation.

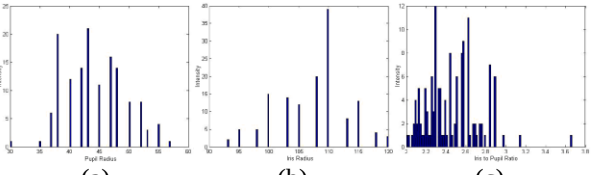

(a) (b) (c)

Fig. 6. Radii histograms: (a) Pupil radii, (b) Iris radii, (c) The ratio of the iris radius to the pupil radius

In this regard, abundance and range of change in the pupil and the iris radii were determined by studying some existing examples of CASIA database [28], and the ratios of these radii were calculated.

$30 \leq$ pupil radius ≤ 60

$90 \leq$ iris radius ≤ 120

$2 \leq$ iris-pupil radius ratio ≤ 3.8

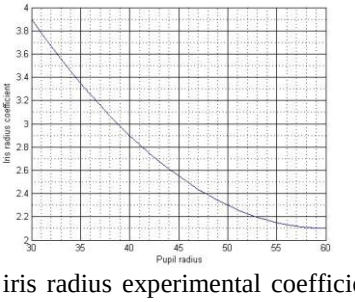

Fig. 7. The iris radius experimental coefficients curve according to the pupil radius; coefficients are considered 0.1 bigger to minimize the possibility of omission of the iris edges.

The experimental results show that the iris radius is almost constant and approximately equal to 110 pixels, while even for a particular eye, the pupil radius is not constant and always differs due to the ambient lighting changes. Thereupon, there is an inverse relationship between the pupil radius and the ratio of two radii; this means that by increasing the radius of the pupil, the

iris-pupil radius ratio will decrease. Based on this fact, the curve above (Figure 7) can be fitted to the experimental results obtained from Hough transform segmentation method and using this curve, iris radius can be approximated from the pupil radius. Approximation is done using equations (16) and (17).

$$C = 0.002(r_p - 60)^2 + 2.1 \quad (16)$$

$$\hat{r}_i = C \times r_p \quad (17)$$

where C is the iris radius coefficient, r_p is the pupil radius and $\hat{r}_i$ is the approximated iris radius.

After pupil localization and by using the approximated iris radius obtained from equation (17), the ROI for the iris outer boundary detection can be determined. The area outside this region usually includes occlusions such as eyelashes or eyelids. These occlusions disrupt the search for the maximum rate of change in both sides of the iris and cause error in the algorithm; thereupon, the brightness of the outer regions is replaced with the average grayscale value of the sclera in each side of the eye by using the vertical line passing through the pupil center as reference. In the next step, long eyelashes or lighting reflections in the ROI are detected using thresholding technique and are also replaced with the average grayscale value of the sclera.

Performing the steps above, a perfectly suitable image for iris localization is obtained and the error probability of detection of the external borders is greatly reduced; now a fast method such as searching for the maximum rate of change can be used for the iris outer border detection. In order to find the left edge, a rectangular area with 20 rows and 10 columns is such assumed that its top left corner is placed horizontally 10 pixels before the estimated iris boundary and vertically 10 pixels below the horizontal line passing through the pupil center. The sum of grayscale values of pixels located within this area is calculated; this rectangle is then shifted one pixel to the right, and the sum of grayscale values is calculated again. Now the difference between these two sums is calculated and is saved; the saved number is actually a measure for comparing changes in brightness between these areas. This procedure continues until the right side of the assumed rectangle reaches to 50 pixels of the pupil boundary. The maximum rate of change indicates entering of the assumed rectangle into the iris region; thereupon, the middle pixel of the horizontal side of this specific rectangle can be considered as a good approximation for the left edge of the iris boundary.

The right edge of the iris is also detected by assuming the rectangular area 10 pixels ahead of the estimated iris boundary in the right side of the eye and shifting it to the left. The radius of the iris and the horizontal coordinate of its center can be calculated using equations (18) and (19), respectively.

$$r_i = \frac{1}{2}(X_r - X_l) \quad (18)$$

$$X_i = X_l + r_i \quad (19)$$

where r_i is the iris radius, X_r and X_l are the horizontal coordinates of the right and the left edge points respectively and X_i is the iris center horizontal coordinate.

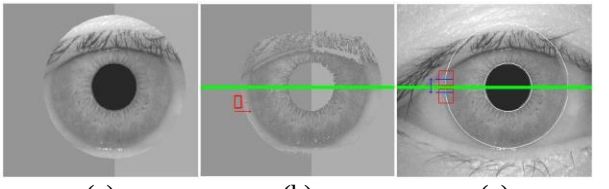

(a) (b) (c)

Fig. 8. Limbic boundary detection: (a) Replacing the brightness of the outer regions with the average grayscale value of the sclera, (b) Detecting the radius and the x-coordinate of the iris center, (c) Detecting the y-coordinate of the iris center

As it has been proven by many experiments, the main difference between the coordinates of the iris center and the pupil center is in the horizontal direction, and the vertical difference between them is usually so minor; thus, the iris center vertical coordinate can be detected by searching around the horizontal line passing through the pupil center. For this purpose, two squares with dimensions of 11 × 11 pixels are assumed at each side of the iris, one above and one below the horizontal line passing through the pupil center; these squares are such assumed that the iris outer boundary passes right through them and divides them into two almost equal areas. Then, the sums of grayscale values are calculated row by row, for all four-square areas; doing so the row with the lowest brightness is identified in each square area. Half the distance between the rows identified in the squares on each side, can be considered as estimation for the vertical coordinate of the iris center. Finally to determine this coordinate more precisely, the average of estimates obtained from each side of the iris is calculated and the result is considered as the y-coordinate of the iris center. This operation is done using equations (20) and (21).

$$\hat{Y} = \frac{1}{2}(Y_b + Y_t) \quad (20)$$

$$Y_i = \frac{1}{2}(\hat{Y}_l + \hat{Y}_r) \quad (21)$$

where Y_b and Y_t are the indices of the bottom, and the top rows identified in the squares on each side of the iris, $\hat{Y}_l$ and $\hat{Y}_r$ are the estimations of the iris center vertical coordinate obtained from the left side and the right side of the eye, respectively, and Y_i is the iris center y-coordinate.

4. EXPERIMENTAL RESULTS

All the experiments were carried out on a system with Intel Pentium M 1.8 GHz processor and 512 MB of RAM using MATLAB 7.8.0 software and CASIA V1.0 [28] eye image database.

To evaluate the accuracy and the speed of the proposed iris localization method, it has been compared to Wildes' segmentation algorithm, which is one of the most accurate methods to locate the iris region. Both methods were used to segment 140 images from the database and both were successfully able to segment all the images with no errors. The average time required for segmenting each image by using Hough transform method is equal to 41 seconds while the proposed method reduces this time to 0.31 seconds.

To assess the segmentation accuracy of the proposed method, two 90 degree cones were selected from both sides of the iris circular region detected by each of the mentioned methods; after remapping the selected pixels into polar coordinates and performing the normalization process, a 60 × 300 pixels template was produced from each eye image.

After performing illumination compensation and contrast enhancement procedures on these templates, their textural characteristics were extracted using cumulative sum based gray change analysis method, and a 9000-bit binary code was produced from each of them; in order to calculate the similarity of iris codes, Hamming distance method was used.

The system which uses Hough transform method for segmentation propose, can correctly identify authorized individuals from impostors with EER equal to 0.95%, when the threshold is 40.14; the second system which takes advantage of the proposed segmentation method, achieves less than 0.24% EER, when the threshold is 40.28. The accuracies of both identification systems are shown in figures 9 and 10.

Then, the proposed method was used in the segmentation of all 756 images from the database. The average elapsed time for detecting the boundary circles of the iris in each eye image is 0.35 seconds, and the algorithm achieves 98.02% accuracy rate. Only in 15 images, the proposed method has some minor errors in detecting the exact boundaries (Figure 11).

Table 1 demonstrates the accuracy rate of the proposed method in compare with the other conventional segmentation techniques.

Table 1. Accuracy rates of iris localization techniques on CASIA database

Methodology	Accuracy rate (%)
Daugman [7]	57.7
Wildes [12]	86.49
Proposed	98.02

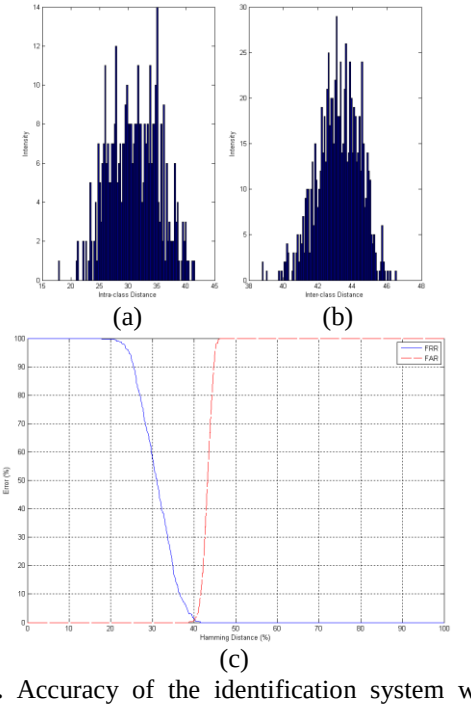

(a) (b) (c)

Fig. 9. Accuracy of the identification system which uses Wildes' segmentation method: (a) Intra-class Hamming distance distribution, (b) Inter-class Hamming distance distribution, (c) FAR/FRR curves according to the Hamming distance

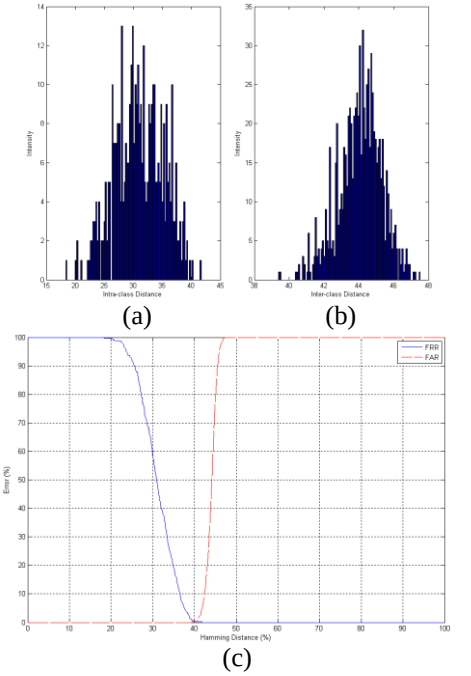

(a) (b) (c)

Fig. 10. Accuracy of the identification system which uses proposed segmentation method: (a) Intra-class Hamming distance distribution, (b) Inter-class Hamming distance distribution, (c) FAR/FRR curves according to the Hamming distance

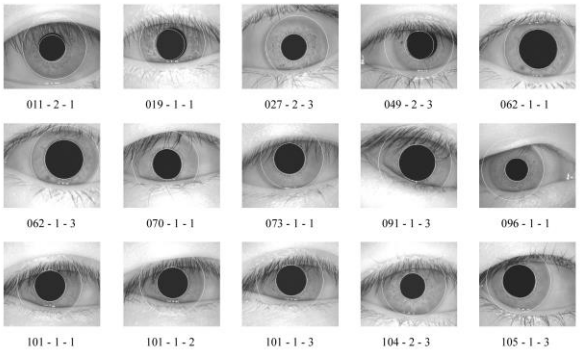

Fig. 11. Inaccurate iris localization

To assess the classification performance of fuzzy ARTMAP network, it has been compared with the Hamming distance method. After detecting the iris region by using the approximated iris radius technique, an 1800-bit binary code was produced from each normalized template as explained previously.

To simulate the real-world application, both systems were trained to identify 60 individuals using all 180 images of subjects captured during the first session; then, the false rejection rate (FRR) was calculated using 240 images of these authorized users captured during the second session. To calculate the false acceptance rate (FAR), the remaining 336 images that belong to unauthorized individuals were used.

The system which uses Hamming distance method for classification, achieves 2.06% EER when the threshold is 35.23; the accuracy of this identification system is shown in figure 12.

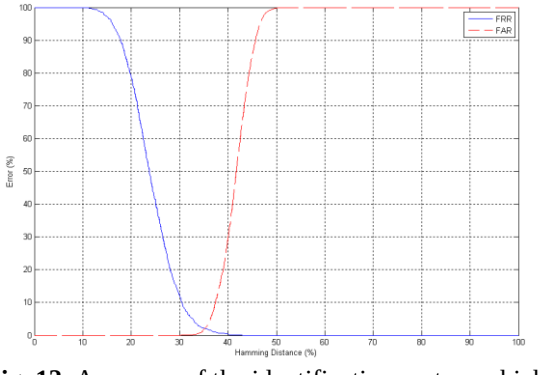

Fig. 12. Accuracy of the identification system which uses Hamming distance classification method

During the training phase, for both ART modules of the system which uses fuzzy ARTMAP network for classification, the learning rate parameter β is considered equal to 1 in order to achieve the fastest learning performance and the choice parameter α is considered equal to 0.001 in order to speed up the selection of the winner category.

During the test phase, the choice parameter of ART_a is remained the same, and the vigilance parameter of this module is such increased that the FAR is reduced to zero; when this goal is achieved, the FRR is also reduced by increasing the number of the training patterns used for each authorized user.

Accordingly, in the first step, a single training image is used for introducing each authorized person to the system; by increasing the vigilance parameter ρ_a to 0.72, FAR is dropped to zero and 32.5% FRR is obtained. Then, the FRR is reduced to 14.17% by using a pair of training images for each user. By using all three images captured in the first session, the FRR is also reduced to zero and a fast, accurate and noise resistant identification system is successfully designed. The accuracy of this identification system according to the vigilance parameter of ART_a is shown in figure 13.

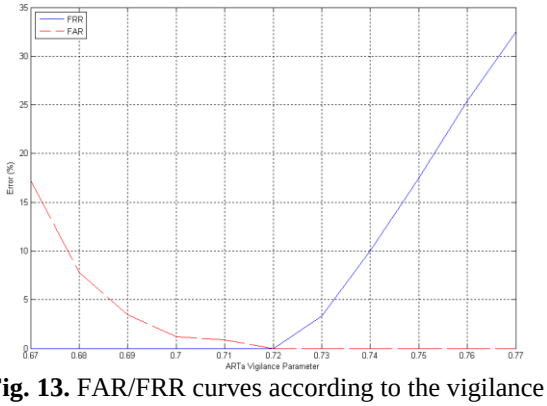

Fig. 13. FAR/FRR curves according to the vigilance parameter of ART_a

The vigilance parameter determines the minimum consistency between the input and the reference code, to be detected as similar patterns. Training result of the ARTMAP network based on applying different vigilance parameters is shown in table 2. By increasing the vigilance parameter during the training phase, the number of categories and thus accuracy of the network classification increases. Thereupon, ρ_a and ρ_b and also ρ_{ab} are considered equal to 1; so, during the training phase, separated classification categories are created in ART modules for each new training pattern. In this mode, the network only refuses to register repetitive patterns.

Table 2. Performance of the system according to the vigilance parameter

Training		Testing		
ART_a Vigilance Parameter	No. ART_a Categories	ART_a Vigilance Parameter	FAR (%)	FRR (%)
0.7	113	0.72	0	86.67
0.8	154	0.72	0	27.5
0.9	179	0.72	0	0
1	180	0.72	0	0

The proposed system can identify all 60 enrolled users with 100% accuracy and without accepting even one unauthorized person. The average time required to perform pre-process and feature extraction procedures for each image is less than 0.37 seconds, and authentication for each input code is almost 10 times faster than the Hamming distance method and takes less than 0.0008 seconds.

Table 3 demonstrates the accuracy rate of the proposed system in compare with the other conventional approaches.

Table 3. Accuracy rates of iris recognition systems on CASIA database

Methodology	Accuracy rate (%)
Boles [15]	92.61
Li Ma [17]	94.33
Wang [21]	97.25
Daugman [6]	99.37
Proposed	100

According to the results shown in table 3 the proposed system has the best identification performance on CASIA database among all the existing methods, clearly.

5. CONCLUSIONS

Most of the calculations in the iris recognition process are related to the segmentation stage; therefore, applying methods with simpler algorithms noticeably increases the speed of the identification system and makes it more suitable for on-line usage. In this paper, a novel method for the accurate and also fast iris localization was proposed. Experimental results show that in compare with an accurate segmentation technique such as Hough transform, the proposed method can detect the iris boundaries approximately 130 times faster as well as reducing the identification system error.

On the other hand, the input images are most likely noisy; thus, the accuracy of the identification system rises using noise resistant feature extraction and classification algorithms such as the cumulative sum based gray change analysis method and fuzzy ARTMAP neural network. Despite its low computational complexity, this feature encoding technique has a very good noise resistance. Fuzzy ARTMAP networks can also classify input patterns correctly even if more than 30% of them have been affected by noise; so, even by using 1800-bit iris codes, which are significantly shorter than those that used in the first set of experiments, the proposed system still achieves the best possible accuracy. Another advantage of this classification method in compare with perceptron based networks is incremental or on-line learning. Therefore, the database of the system can be quickly edited without performing a time-consuming off-line learning process.

The results of simulations on CASIA iris database illustrate that a fast, accurate and noise resistant personal identification system has been successfully designed by using a combination of the mentioned methods. However, in future studies, it is necessary to do experiments on more eye image databases to make the iris recognition system more reliable.

REFERENCES

[1] A. Jain, R. Bolle, S. Pankanti, **"Biometrics: Personal Identification in a Networked Society,"** *Kluwer Academic Publishers*, 1999.

[2] F. Adler, **"Physiology of the Eye: Clinical Application,"** *Fourth edition London: The C.V. Mosby Company*, 1965.

[3] John G. Daugman, **"Biometric Personal Identification System Based on Iris Analysis,"** *US Patent*, no. 5291560, 1994.

[4] M. Gopikrishnan, T. Santhanam, **"Neural Network Based Accurate Biometric Recognition and Identification of Human Iris Patterns,"** *Journal of Computer Science*, vol. 6, no. 10, pp. 1170-1173, 2010.

[5] Rahib H. Abiyev, Koray Altunkaya, **"Personal Iris Recognition Using Neural Network,"** *International Journal of Security and its Applications*, vol. 2, no. 2, pp. 41-50, April 2008.

[6] John G. Daugman, **"High Confidence Visual Recognition of Persons by a Test of Statistical Independence,"** *IEEE Transactions on Pattern Analysis and Machine Intelligence*, vol. 15, no. 11, pp. 1148-1161, 1993.

[7] John G. Daugman, C. Downing, **"Recognizing iris texture by phase demodulation,"** *IEEE Colloquium on Image Processing for Biometric Measurement*, vol. 2, pp. 1-8, 1994.

[8] John G. Daugman, **"Statistical Richness of Visual Phase Information: Update on Recognizing Persons by Iris Patterns,"** *International Journal of Computer Vision*, vol. 45, no. 1, pp. 25-38, 2001.

[9] John G. Daugman, **"Demodulation by Complex-Valued Wavelets for Stochastic Pattern Recognition,"** *International Journal of Wavelets, Multi resolution and Information Processing*, vol. 1, no. 1, pp. 1-17, 2003.

[10] John G. Daugman, **"How iris recognition works,"** *IEEE Transactions on Circuits and Systems for Video Technology*, vol. 14, pp. 21-30, January 2004.

[11] Libor Masek, **"Recognition of Human Iris Patterns for Biometric Identification,"** *Report for Bachelor of Engineering degree, Presented to the School of Computer Science and Software Engineering, The University of Western Australia*, 2003.

[12] R. Wildes, J. Asmuth, G. Green, S. Hsu, R. Kolczynski, J. Matey, S. McBride, **"A Machine-Vision System for Iris Recognition,"** *Machine Vision and Applications*, vol. 9, pp. 1-8, 1996.

[13] R. Wildes, **"Iris Recognition: An emerging Biometric Technology,"** *IEEE Proceedings*, vol. 46,

no. 4, pp. 1185-1188, 1998.

[14] Li Ma, Y. H. Wang, T. N. Tan, **"Iris recognition based on multichannel Gabor filtering,"** *Proceedings of the Fifth Asian Conference on Computer Vision, Australia*, pp. 279-283, 2002.

[15] W. Boles, B. Boashash, **"A Human Identification Technique Using Images of the Iris and Wavelet Transform,"** *IEEE Transactions on Signal Processing*, vol. 46, no. 4, pp. 1185-1188, 1998.

[16] C. Sanchez-Avila, R. Sanchez-Reillo, **"Iris-Based Biometric Recognition Using Dyadic Wavelet Transform,"** *IEEE Aerospace and Electronic Systems Magazine*, pp. 3-6, 2002.

[17] Li Ma, Tieniu Tan, Yunhong Wang, Dexin Zhang, **"Personal Identification Based on Iris Texture Analysis,"** *IEEE Transaction on Pattern Analysis and Machine Intelligence*, vol. 25, no. 12, 2003.

[18] S. Lim, K. Lee, O. Byeon, T. Kim, **"Efficient Iris Recognition through Improvement of Feature Vector and Classifier,"** *ETRI Journal*, vol. 23, no. 2, pp. 61-70, 2001.

[19] C. Tisse, L. Martin, L. Torres, M. Robert, **"Person Identification Technique Using Human Iris Recognition,"** *Proceedings of Vision Interface*, pp. 294-299, 2002.

[20] Ya-Ping Huang, Si-Wei Luo, En-Yi Chen, **"An Efficient Iris Recognition System,"** *Proceedings of the First International Conference on Machine Learning and Cybernetics, Beijing*, November 2003.

[21] Yong Wang, Jiu-Qiang Han, **"Iris Recognition Using Independent Component Analysis,"** *Proceedings of the Fourth International Conference on Machine Learning and Cybernetics*, Guangzhou, 2005.

[22] V. Dorairaj, N. Schmid, G. Fahmy, **"Performance Evaluation of Iris Based Recognition System Implementing PCA and ICA Techniques,"** *Proceedings of SPIE 2005 Symposium, Orlando*, 2005.

[23] Michael J. Brown, **"Singular Value Decomposition & 2D Principal Component Analysis of Iris Biometrics for Automatic Human Identification,"** *Master of Science Thesis, Presented to Russ College of Engineering & Technology, Ohio University*, June 2006.

[24] Jong Gook Ko, Youn Hee Gil, Jang Hee Yoo, Il Chung, **"Method of Iris Recognition using Cumulative-Sum-Based Change Point Analysis and Apparatus using the same,"** *U.S. Patent Application Publication*, Pub. no.: US 0014438 A1, January 2007.

[25] Jong Gook Ko, Youn Hee Gil, Jang Hee Yoo, Il Chung, **"A Novel and Efficient Feature Extraction Method for Iris Recognition,"** *ETRI Journal*, vol. 29, no. 3, pp. 399- 401, June 2007.

[26] Gail A. Carpenter, Stephen Grossberg, Natalya Markuzon, John H. Reynolds, David B. Rosen, **"Fuzzy ARTMAP: A Neural Network Architecture for Incremental Supervised Learning of Analog Multidimensional Maps,"** *IEEE Transactions on Neural Networks*, vol. 3, no. 5, pp. 698-713, September 1992.

[27] Gail A. Carpenter, Stephen Grossberg, John H. Reynolds, **"Fuzzy ARTMAP, Slow Learning, and Probability Estimation,"** *Boston University Center for Adaptive Systems and Department of Cognitive and Neural Systems*, January 1993.

[28] Center for Biometrics and Security Research, Institute of Automation, Chinese Academy of Sciences. Iris Image Database (CASIA V1.0) http://www.cbsr.ia.ac.cn/IrisDatabase.htm, Accessed June 2011.